In-situ redox cycling behavior of Ni-$BaZr_{0.85}Y_{0.15}O_{3-\delta}$ cermet anodes for Protonic Ceramic Fuel Cells

Nasani Narendar[1], Zhu-Jun Wang[2], Marc G. Willinger[2], Aleksey A. Yaremchenko[3], Duncan P. Fagg[1]*

[1]Nanotechnology Research Division, Centre for Mechanical Technology and Automation, Department of Mechanical Engineering, University of Aveiro, 3810-193 Aveiro, Portugal.

[2]Department of Inorganic Chemistry, Fritz Haber Institute of the Max Planck Society, Faradayweg 4-6, D-12489 Berlin, Germany.

[3]Department of Materials and Ceramic Engineering, CICECO, University of Aveiro, 3810 193, Aveiro, Portugal.

*: Corresponding author, E-mail: duncan@ua.pt; Fax: +351-234-370953;

Tel: +351-234-370830

Abstract: The current work investigates the redox behaviour of peak performing Ni-$BaZr_{0.85}Y_{0.15}O_{3-\delta}$ (Ni-BZY) cermet anodes for protonic ceramic fuel cells (PCFCs) by electrochemical impedance measurements, scanning electron microscopy (SEM) and X-ray diffraction (XRD). Peak performing PCFC cermet anodes are documented to require much lower porosity levels than those needed in oxide-ion conducting counterparts. The polarisation behaviour of these optimised PCFC anodes is shown to be drastically impaired by redox cycling, with depletions in performance that correspond to around 80% of the original resistance values noted after the first redox cycle. The ohmic resistance (Rohmic) is also shown to be increased due to delamination at the electrode/electrolyte interface, as confirmed by postmortem microstructural analysis. In-situ measurements by environmental scanning microscopy (ESEM) reveal that degradation proceeds due to volume expansion of the nickel phase during the re-oxidation stage of redox cycling. The present study reveals degradation to be very fast for peak performing Ni-BZY cermets of low porosity. Hence, methods to improve redox stability can be considered to be essential before such anodes can be implemented in practical devices.

Keywords: Protonic ceramic fuel cells (PCFC); redox cycling; Ni-cermet anodes; polarization behavior; environmental scanning microscopy (ESEM); Barium Zirconate

1. Introduction

Protonic ceramic fuel cells (PCFC) are of great interest for conversion of chemical energy into electrical energy with high efficiency and low levels of pollution [1]. The high-temperature protonconductors formed from acceptor doped $BaCeO_3$, $BaZrO_3$ or mixed solid solutions of $BaCeO_3$ and $BaZrO_3$, are promising electrolytes for intermediate-temperature (400-700 °C) solid oxide fuel cells (IT-SOFCs) due to their greater ionic conductivities at these temperatures as compared to conventional oxide-ion conducting electrolytes [2, 3]. PCFCs offer the flexibility that they can be operated with a wide range of potential fuels such as hydrocarbons, methanol and ammonia etc. [4]. Furthermore, in comparison to oxide-ion conducting ceramic fuel cells, PCFCs offer the important advantage of non-dilution of fuel during operation, as water vapour is formed at the cathode.

For PCFCs, the potential anode materials Ni-$Ba(Ce,Y)O_{3-\delta}$ (Ni-BCY) [5, 6], Ni-$Ba(Zr,Y)O_{3-\delta}$ (Ni-BZY) [7], $Ba(Ce,Zr,Y,Yb)O_{3-\delta}$ [8], Ni-$SrCe_{0.9}Yb_{0.1}O_{3-\delta}$ [9] $Ca(Zr,Y)O_{3-\delta}$, Ni-$Sr(Zr,Y)O_{3-\delta}$ [10] and Ni-$Ba(Ce,Zr,Y)O_{3-\delta}$ [11-14] have been reported in the literature. Due to the instability of BCY in H_2O and CO_2 containing atmospheres, cermet anodes of Ni-BCY may be unsuitable for practical operation in alternative carbonaceous fuels [4]. On the contrary, BZY shows better chemical stability in H_2O and CO_2 containing atmospheres and, hence, may be the more promising component for the anode cermet matrix in these devices.

Recently, a novel synthesis route to form Ni-BZY cermets and their resultant electrochemical behavior has been documented by the current authors [15]. Our previous studies and further works in the literature, have shown the area specific resistance (ASR) of Ni-BZY to be within the suitable range <1.5 Ω cm^2 for efficient

fuel cell operation [7, 15]. The performance of PCFC cermet anodes has been shown to be tailorable by changes in the Ni content, the proton conductivity of the ceramic matrix phase [7] and the porosity [8]. Nonetheless, to date, none of these optimized anode materials have been tested in long-term fuel cell operation, where the robustness of PCFC systems will be strongly impacted by real operating conditions that may include system shutdown, interruption of fuel supply, fluctuating power demand and minor seal leakage; factors that have commonly been shown to lead to degradation of performance in oxide-ion conducting SOFCs [16]. In addition, many ceramic proton conductors have been reported to offer mixed transport for both protons and oxide-ions [17]. In such a case, steam may permeate through the membrane upon the existence of a water vapor partial pressure gradient. This effect has been described for a PCFC, where the water vapor partial pressure of the exhaust is commonly an order of magnitude higher than the fuel atmosphere [17]. This gradient provides a large driving force for steam permeation to the anode compartment that may have negative impact on the anode stability by potential nickel oxidation.

In order to achieve a high electrochemical performance, anode cermets should possess a long triple phase boundary (TPB) (between the metallic phase, ceramic phase and gas phase) to maximize electrochemical reactions. However, it is well-known that redox cycling can adversely affect the TPB length [18]. The redox behavior of state-of-the-art Ni-YSZ anodes for oxygen-ion conducting fuel cells has been well documented in the literature [18-21] with several authors noting that the original microstructure and phase distribution cannot be restored when re-oxidation and re-reduction take place [18, 20, 22, 23]. Moreover, previous studies have shown that the durability of anodes is critically dependent on their microstructure and the cermet phase distribution [16, 24].

The available data highlight that Ni-YSZ is strongly affected by redox cycling and that the degradation rate of the cell can be very fast, especially at low porosity. Re-oxidation of Ni to NiO leads to a bulk volume expansion of the cermet, which commonly causes micro-cracks and also delamination at the electrode/electrolyte interface; factors that reduce the fuel cell performance [16, 25].

To date there has been no literature data available on the redox behavior of PCFC cermet anodes. Moreover, due to some unique features of PCFC anodes, their redox tolerance may differ radically in comparison to their oxide-ion conducting counterparts. Firstly, in a PCFC cermet anode both the Ni phase and the ceramic oxide matrix phase can offer proton conductivity. This unique factor has led authors to state that a PCFC cermet anode may have a lower dependence on the three-phase-boundary length than an oxide-ion conducting counterpart, due to the high mobility of protons through both the metallic nickel phase and the ceramic matrix [26]. As such, this factor may lead to lower performance degradation upon alteration of the microstructure (thus, three phase boundary length) during redox cycling. On the other hand, it has also been noted that lower porosity is desirable to obtain peak performance in PCFC anodes (as hydrogen is the only diffusing gas species), in contrast to that of an oxide-ion conducting anode in which water vapour must also counter-diffuse [8, 15, 27]. This second factor may produce a very serious negative effect on redox cycling stability, as it has been noted that a higher porosity is preferable to minimize bulk volume expansion upon Ni re-oxidation in oxide-ion conducting cermets [28]. Hence, these unique features may radically alter the redox tolerance of PCFC anodes, in contrast to their oxide-ion conducting counterparts.

Thus, we herein report the degradation of peak performing 40vol% Ni-BZY anodes, of low porosity, by redox cycling using electrochemical impedance measurements, SEM and in-situ ESEM techniques. The content of 40vol%Ni was selected as it represented the lowest Ni content required to ensure percolation [15]. The redox cycles were performed on a Ni-BZY/BCZY/Ni-BZY symmetrical cell, cycling between a 10% H_2/N_2 gas mixture and an air stream.

2. Experimental

2.1 Synthesis of Ni-BZY cermet and formation of electrochemical samples.

NiO-BZY anodes (40 vol% Ni) were prepared by dispersing nickel in pre-made BZY by the method of microwave-assisted combustion, using a new acetate-H_2O_2 based route [15]. The $BaZr_{0.85}Y_{0.15}O_{3-\delta}$ powder was pre-prepared by mechanosynthesis, as described in the literature [29]. $Ni(OCOCH_3)_2.4H_2O$ (Aldrich, 99% pure) and 30% H_2O_2 (Riedel-de Haen, 30% by weight) were used for the combustion reaction to disperse the nickel phase in the pre-made BZY to form the cermet material. A stoichiometric amount of nickel acetate was dissolved in distilled water, and the pre-prepared BZY was dispersed using an ultrasonic bath. An appropriate amount of 30% H_2O_2 was then slowly added, fixing the fuel to oxidant ratio of nickel acetate/H_2O_2 to 1:1, according to the propellant chemistry. The solution was heated on a hot plate at 80 °C until a viscous gel formed. The viscous gel was then heated and simultaneously rotated in a domestic 2.45 GHz, 800W microwave oven set at the maximum power. After a few minutes, the dried gel burned with a flame in a self-propagating combustion manner, releasing plentiful fumes until the gels were completely burned to form a black powder. The powder was calcined at 1400 °C for 5h in ambient air for XRD phase analysis.

For electrochemical measurements disc shaped, symmetrical Ni-BZY/BCZY/Ni-BZY, anode/electrolyte/anode, assemblies were fabricated by the co-pressing technique as described in our previous work [15]. First, $BaCe_{0.7}Zr_{0.1}Y_{0.2}O_{3-\delta}$ (BCZY71) electrolyte powder [30] was lightly uniaxially pressed in a 18 mm diameter mould under a pressure of 50 MPa. Then the green NiO-BZY combusted powder (prepared by the acetate-H_2O_2 combustion method) was deposited manually on one side of BCZY substrate, pressed at 100 MPa, and then repeated on the other side with slightly higher pressure of 150 MPa. The resultant symmetrical trilayer assemblies were isostatically pressed at 200 MPa for 5 min and sintered at 1400 °C for 6 h with a heating and cooling rate of 2 °C/min. Isostatic pressing was used to achieve good adherence between anode and electrolyte layer. The sintered trilayer symmetrical cell diameter was ~16mm and the thicknesses of the Ni-BZY anodes were ~110 μm. These anodes were formed without the presence of any porogen, as a low porosity has been shown to be desirable to obtain peak performance in PCFC anodes [8, 27].

2.2 Redox cycling experimental procedure

The redox cycling experiments were performed at 800 °C. The cermet was first reduced in flowing 10% H_2/N_2 gas mixture and then re-oxidized in air. Before every redox cycle the symmetrical cell was maintained in the 10% H_2/N_2 gas mixture and thermally cycled between 800 ºC and 600 ºC, during which impedance measurements were performed. The redox cycling was repeated during the tests according to the steps shown in Fig. 1.

a) The symmetrical cell was reduced at 800 °C in moist 10% H_2/N_2 gas mixture (pH_2O = ~0.031 atm and pO_2 = ~$2.8*10^{-20}$ atm) for 6 hours.

b) The 10% H_2/N_2 gas flow was stopped and the cell purged with N_2 gas for 5 min.

c) For the re-oxidation experiment, the N_2 gas flow was stopped and synthetic air ($80\%N_2/20\%O_2$) was passed for 4 hours.

d) The air flow was stopped and the cell purged with N_2 gas for 5 min.

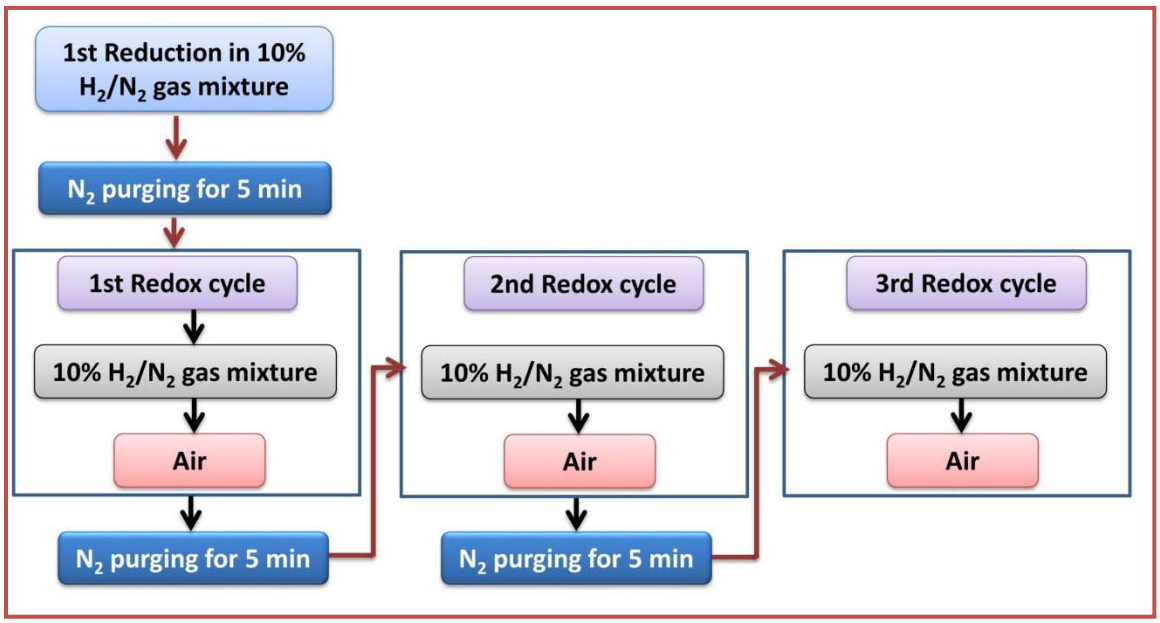

Figure 1: Redox cycling flow chart where one redox cycling consists of (a) the re-oxidation step in air (b) N_2 purging for 5 min and (c) the re-reduction step in 10% H_2/N_2 gas mixture.

2.3. Materials Characterization

X-ray diffraction (XRD) analysis was used to identify the phase purity and the cell parameters of resultant powders in the 2θ range between 20° and 85° using a Rigaku Geigerflex diffractometer (CuKα radiation, scan rate 1°/min). A Scanning Electron Microscope (SEM), model Hitachi SU-70, was used to investigate the microstructure of the pellets before and after the complete redox cycling experiment. *In-situ* ESEM analysis was performed using a FEI Quanta 200 SEM. For the ESEM investigation, an identical Ni-BZY/BCZY/Ni-BZY symmetrical cell was fractured in order to access the electrode/electrolyte interface. Redox cycling was performed at 600 °C under flow of 3 sccm of pure H_2 or O_2 at a total pressure of 2.0 x 10^{-2} Pa to provide complementary dynamic information on redox cycling.

2.4 Electrochemical impedance measurements

Before each redox cycle step, electrochemical impedance measurements were performed to evaluate the performance degradation of the cermet anode. Impedance spectroscopy was performed using an Electrochemie-Autolab PGSTAT302N frequency response analyser in the frequency range of 1 MHz-0.01 Hz, at amplitude of 50 mV. Thermal cycling measurements were made at 50 ºC intervals in the direction of decreasing temperature in the temperature range between 800 and 600 °C. Stability was confirmed by performing repeated impedance measurements at each temperature under moist 10% H_2/N_2, with a flow rate of 50 ml/min. Humidification was obtained by bubbling gases through water followed by a saturated KCl solution in contact with solid KCl, producing approximately 86% relative humidity at room temperature. Humidity levels were measured using a humidity meter (Jumo). The impedance spectra were fitted using the ZView software (Scribner Associates).

3. Results and Discussion

3.1 Phase analysis:

Complete reduction of the precursor NiO-BZY anode to the Ni-BZY cermet was performed in 10% H_2/N_2 mixture at 800 °C for 6 h. Subsequent re-oxidation of anode was accomplished in ambient air at 800 °C for 4h. The XRD patterns of the as-sintered NiO-BZY anode and those measured after first reduction and re-oxidation steps are shown in Fig. 2. All the patterns exhibit the pure perovskite BZY phase, accompanied by NiO for the as-sintered and re-oxidized samples and the Ni phase for the reduced cermet. After re-oxidation the absence of the Ni phase indicates that complete re-oxidation had occurred. Hence, complete Ni redox cycling is accomplished during each redox step, in agreement with the measured oxygen partial pressures during the reduction step, which were shown from oxygen sensor readings to be $10^{-19.5}$-10^{-24} atm in

the temperature range 800 ºC-600 ºC. These values are significantly more reducing than the values required for NiO reduction from a thermodynamic perspective, $pO_2 = 10^{-14}$-10^{-19} atm respectively, in the same temperature range [31]. The perovskite BZY phase was shown to be unaffected during redox cycling.

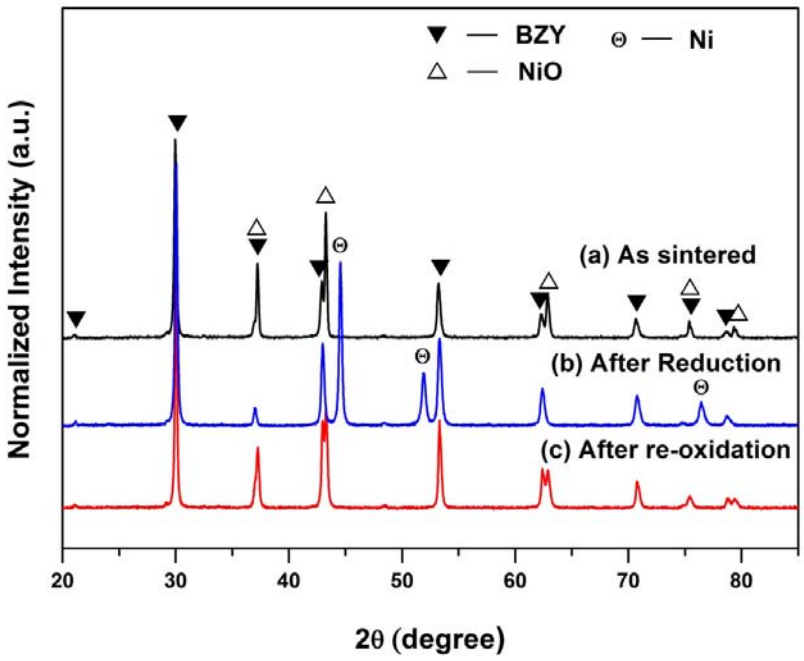

Figure 2: XRD patterns for 40 vol% Ni-BZY cermet anode (a) as sintered (b) after reduction for 6 h and (c) after re-oxidation for 4h.

3.2 Microstructural analysis

Fig. 3 (a) shows the SEM micrographs of the Ni-BZY/BCZY71 interface after initial reduction at 800 °C in 10% H_2/N_2 gas mixture before the redox cycling experiment. No delamination or cracks can be observed at the anode/electrolyte interface. However, after 3 redox cycles, serious delamination is shown to have occurred at the anode/electrolyte interface, Fig. 3 (b). The contact between electrolyte and anode has partially been lost, damaging the area of electrical contact with the electrolyte. In addition, micro cracks in the BZY network and across the anode can be observed after the third redox cycle as shown in surface images of the anode in Fig. 3 (c) and 3 (d).

These factors can be expected to significantly deteriorate the electrochemical cell performance. During real life PCFC operation, the cermet anode may have to support several re-oxidation and reduction cycles [23]. However, the current investigation shows that, even with only 3 redox cycles, rapid microstructural degradation has occurred. To investigate the origin of this phenomenon, complementary information is provided by *in-situ* measurements made with the environmental scanning electron microscope (ESEM).

3.3 ESEM analysis

For the ESEM investigation, the sintered symmetrical cell was fractured in order to access the electrode/electrolyte interface. Typical redox cycling was performed at 600 °C under flowing pure H_2 (3 sccm) or O_2 at a total pressure of 2.0 x 10^{-2} Pa to provide complementary dynamic information on redox cycling. Fig. 4a shows the anode material in its initial reduced state. An intimate and homogenous distribution between the ceramic BZY and Ni metal phases can be observed. The darker particles are those of Ni metal, which present a pocketed microstructure containing very fine porosity. Such fine pores in PCFC anodes were previously measured by mercury intrusion porosimetry to be in the nanometer scale with high surface area [13]. The presence of larger pores of ~0.3-0.7μm has also been noted in reduced PCFC anodes and attributed to channels formed between the Ni grains and the ceramic matrix. These larger pores result from an overall volume contraction of the nickel particle, associated with NiO reduction to Ni metal. Similar channels can be readily seen in Fig. 4a, where the dark Ni particles appear to have pulled away from the lighter coloured BZY matrix. Upon re-oxidation after 10 min., Fig. 4(b), the Ni particles are observed to increase in size, losing some of their fine pocketed structure and closing channels that were previously present between

the Ni phase and the BZY ceramic backbone. Upon re-oxidation to NiO, Fig. 4(c), the NiO particles now, not only completely fill the available voids in the BZY backbone, but also appear to mushroom outwards as their volume extends beyond the available space in the original BZY matrix, Fig. 4(c). The maximum volume of the NiO particle is achieved after approximately 2 hours in these conditions. Such extended growth of Ni particles agrees with that previously noted in oxide-ion conducting Ni-YSZ cermets, where an initial volume change due to NiO reduction (~40%) is significantly exceeded on subsequent re-oxidation (~66%) due to the so called pseudo Kirkendall effect [32]. This phenomenon occurs due to the faster outward diffusion of nickel cations than the inward diffusion of oxide-ions, leading to the creation of internal porosity that produces NiO particles of a larger overall volume. Upon re-reduction, the Ni particles reduce in size once more, pulling away from the BZY backbone and reforming their pocketed appearance, Fig. 4(d,e).

The greater volume change noted for the Ni-particles upon re-oxidation than reduction is a phenomenon that has been reported to be undesirable in Ni-YSZ cermets due to expansion of the cermet anode and delamination of the electrolyte/electrode layer and/or potential cracking of the YSZ backbone [32]. Moreover, these effects have been reported to be more prolific in Ni-YSZ anodes of low porosity [28, 32]. In this respect, PCFC anodes have been reported to offer the highest electrochemical performance at the lowest porosities [8, 27]; a factor that is in direct conflict with the aforementioned criterion for redox stability. The PCFC anodes in the current work were formed without the use of additional porogens and correspond to peak electrochemically performing cermets with final porosity levels of ~34% [8, 33]. This value is much lower than that of state of the art oxide-ion conducing SOFC anodes, which typically contain porosity

levels ~50% [34]. Nonetheless, the current ESEM analysis of PCFC anodes reveals a similar expansion of the NiO particles upon re-oxidation as documented for oxide-ion conducting Ni-YSZ anodes. Consequently, the low porosity PCFC anodes present undesirable microstructural damage upon redox cycling, with extensive degradation phenomena of electrolyte/electrode delamination and fracture of the BZY matrix, as noted in the postmortem SEM images of redox cycled BZY-Ni anodes in the previous section. This degradation is also shown to be very rapid, occurring after only a few redox cycles. Thus, the salient question is if such microstructural damage will lead to serious impairment of the electrochemical properties of PCFC anodes, or if the aforementioned property of ionic transport in both the ceramic and metallic phases of a PCFC cermet anode (and associated extension of the three phase boundary length), as well as a higher initial interconnectivity can offset this microstructural degradation.

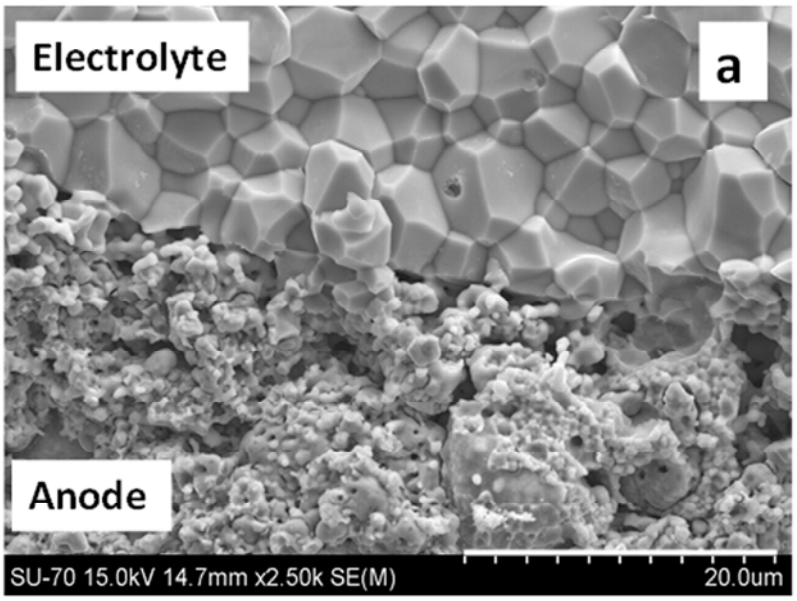
Electrolyte
a
Anode
SU-70 15.0kV 14.7mm x2.50k SE(M)
20.0um

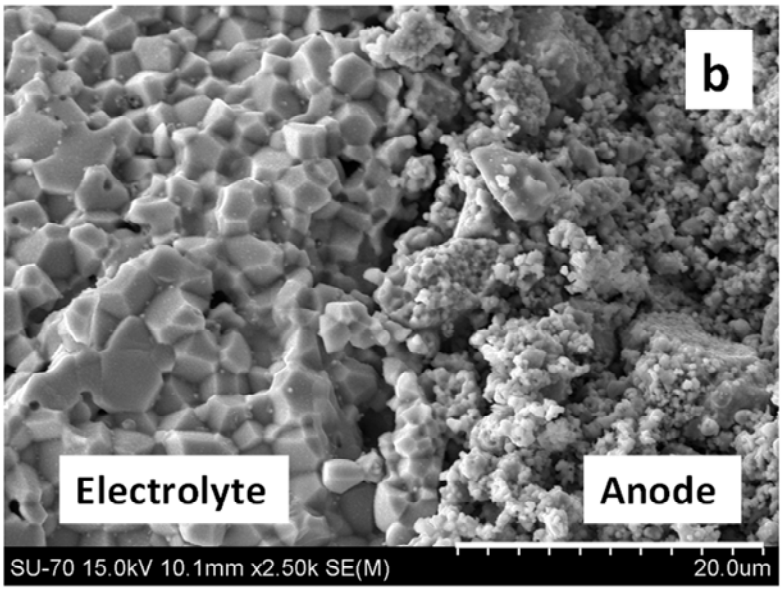
b
Electrolyte
Anode
SU-70 15.0kV 10.1mm x2.50k SE(M)
20.0um

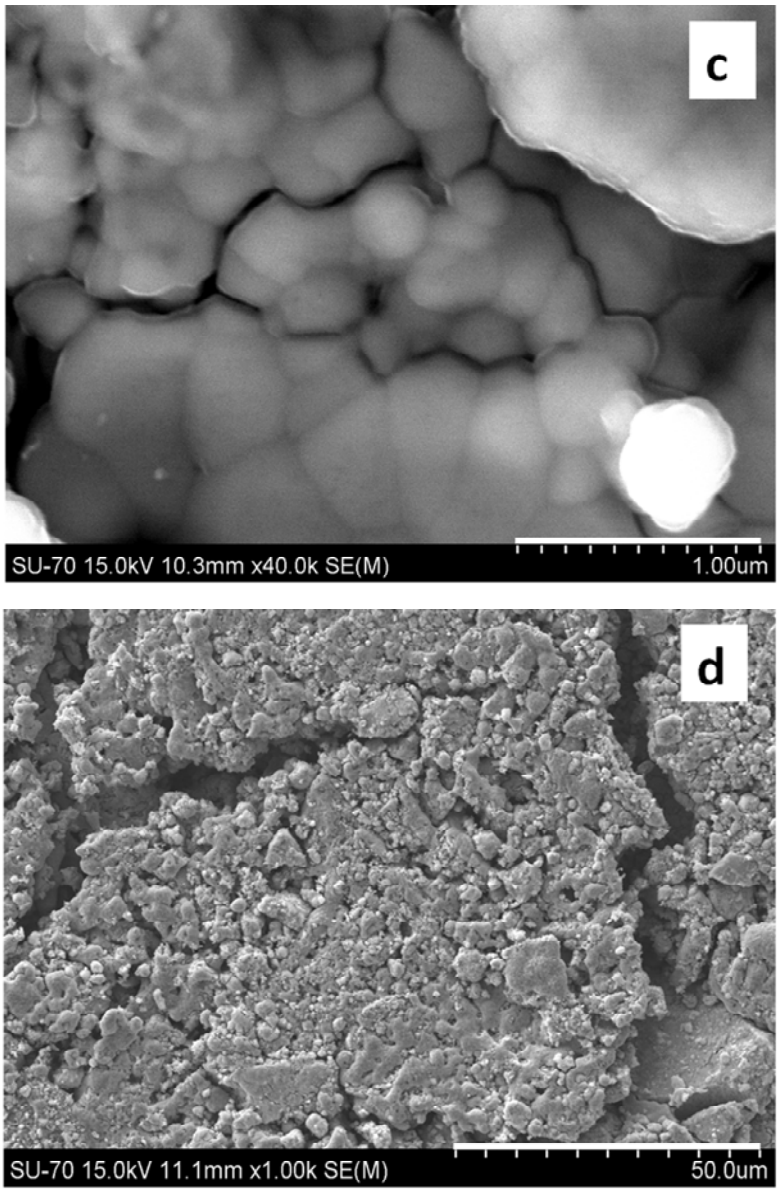

Figure 3: SEM micrographs of (a) cross-sectional anode/electrolyte interface before redox cycle, (b) after three redox cycles, and (c,d) surface images of the anode after 3rd redox cycle

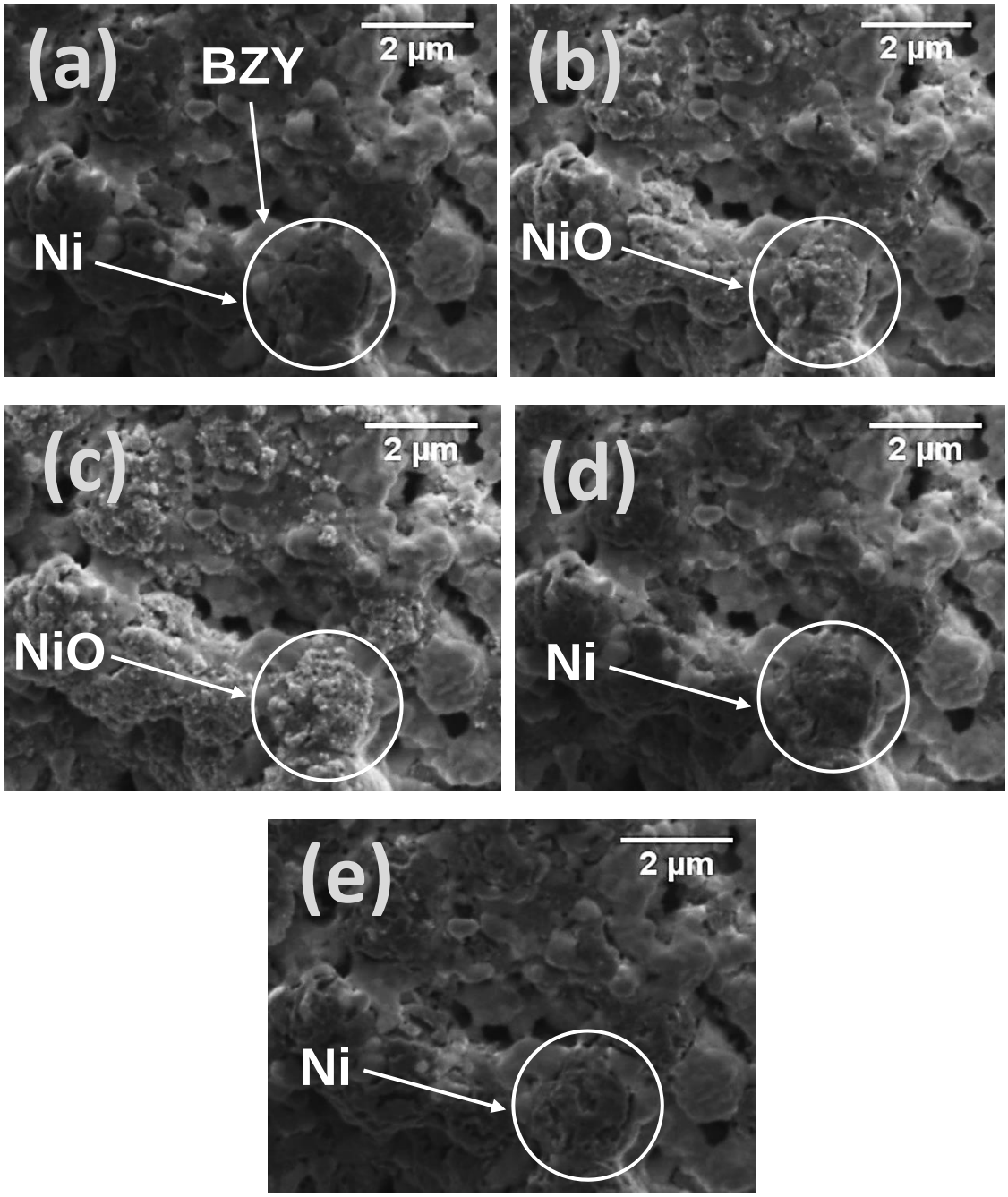

Figure 4: ESEM micrographs of Ni-BZY anode (a) first reduced state, (b) re-oxidation after 10 min, (c) re-oxidised anode after 120 mins (Ni volume expansion is clearly visible upon re-oxidation), (d) re-reduced after 10 min and (e) re-reduced anode after 180 mins.

3.4 Effect of Redox cycling on polarization resistance of Ni-BZY anode

Analysis of the effect of redox cycling on polarization resistance was carried out by impedance spectroscopy using an anode/electrolyte/anode symmetrical cell. The impedance spectra were recorded before each redox cycle in reducing conditions. All

measured impedance spectra from 800 °C-650 °C consist of an offset along the real axis, an inductance effect at high frequency and two depressed semi circles at lower frequencies. An example spectrum is presented at 600 °C, in Fig. 5; all measured spectra were similar in form. The two semi circles observable at lower frequencies are clearly separated from each other and represent two distinct electrochemical reactions occurring at the anode. The impedance diagrams were, therefore, analyzed by using an equivalent circuit comprising of an inductance in series with a resistor, R, and two distributed RQ elements, as shown in the inset of Fig. 5. The fitting parameters extracted for each distributed semicircle are the resistance, R, the pseudo-capacitance, Q, and an additional parameter n which can be related to the true capacitance by the equation

$$C = R^{(1-n)/n} Q^{1/n} \qquad (1)$$

In this way, the true capacitance values of the distributed responses have been calculated to be in the order of 10^{-5}-10^{-6} Fcm^{-2} for the higher frequency response, associated with resistance R2, and 10^{-3}-10^{-4} Fcm^{-2} for the lower frequency response, associated with resistance R3. The obtained capacitance values correspond well to those previously noted for Ni-BZY electrodes [7, 15].

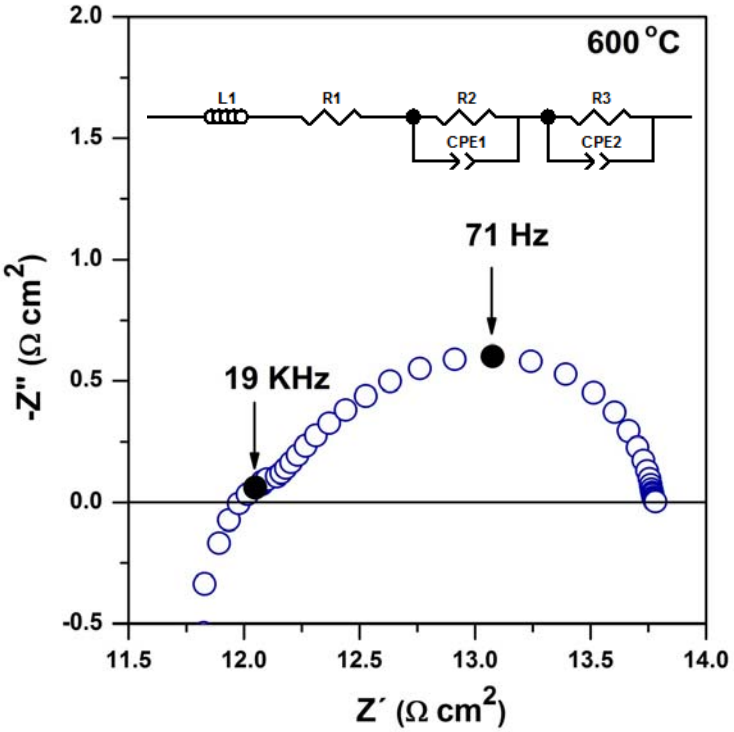

Figure 5: The electrochemical impedance spectrum of a symmetrical cell with 40 vol% Ni-BZY electrode, measured in wet 10% H_2/N_2 at 600 °C.

The higher frequency semicircle (R2) and the lower frequency semicircle (R3) were attributed to the polarization resistance of the PCFC anode, Rp = R2 +R3, as in our previous works [15], while the high frequency intercept (R1) was associated with the ohmic resistance of the symmetrical cell.

Upon redox cycling the overall shapes of the impedance spectra remain similar, while each term in the impedance spectra, R1, R2 and R3, are shown to increase in resistance, Fig. 6.

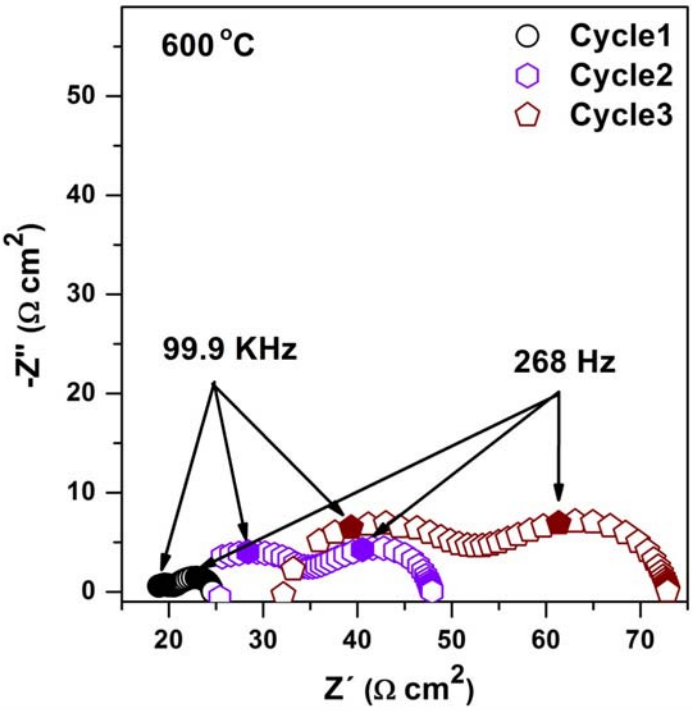

Figure 6: The effect of redox cycling on impedance spectra for 40 vol% Ni-BZY cermet anode measured in wet 10% H_2/N_2 at 600 ºC.

Fig. 7 shows the total polarization resistance Rp of Ni-BZY cermet as a function of temperature for each redox cycle. The results show that Rp increases dramatically from the first redox cycle to third redox cycle, in agreement with Fig. 6. To investigate the detailed electrochemical degradation of Ni-BZY upon redox cycling, total polarization resistance was separated into each contribution, R2 and R3. The high frequency polarization resistance R2 and low frequency polarization resistance R3 were plotted as a function of temperature as shown in Fig. 8(a) and 8(b). Both polarization resistances R2 and R3 are substantially affected by redox cycling. After the 1st redox cycle R2 and R3 increase and continue to increase with each redox cycle, as one can observe in fig. 8(a) and 8(b). The high frequency response, R2, was the most highly affected term, as compared to R3. This is consistent with previous results reported for Ni-BZY, which showed the R2 term to be predominately a microstructural dependent term related to the three phase boundary length [27] where the presence of microcracks would be expected

to have a negative impact. Similarly, a decrease in the three phase boundary length would be expected on loss of connectivity between the BZY matrix and the Ni phase, or due to depleted interconnectivity within the Ni and BZY networks [16, 20]. Fig. 8(c) depicts the ohmic resistance (Rohmic) as a function of temperature. After each redox cycle the Rohmic of the symmetrical cell was also significantly increased. From the microscopy study, delamination occurs with redox cycling at the anode/electrolyte interface, (Fig. 3(b) and Fig. 3(c)). Hence, the increase in ohmic resistance appears to result from the observed delamination at the anode/electrolyte interfaces and the associated increase in contact resistance.

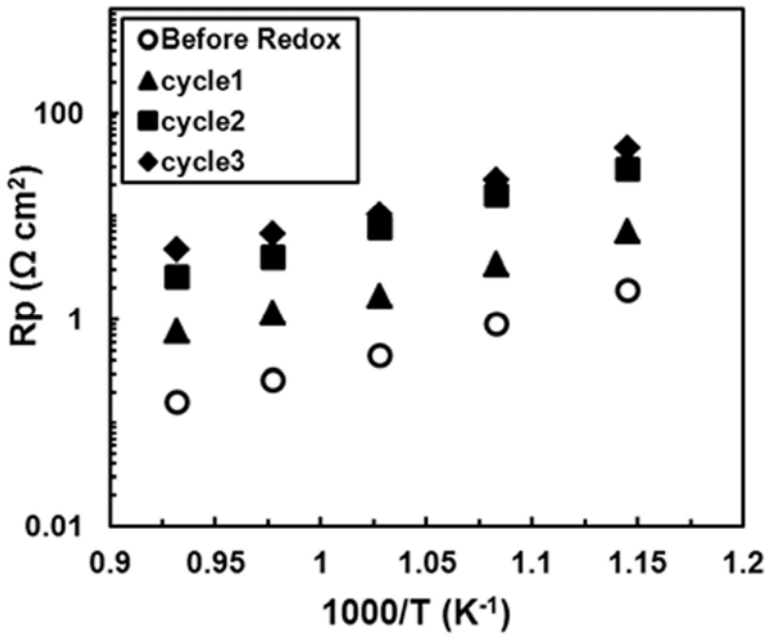

Figure 7: The effect of redox cycling on total polarization resistance (Rp) as a function of temperature for 40 vol% Ni-BZY cermet anode measured in wet 10% H_2/N_2.

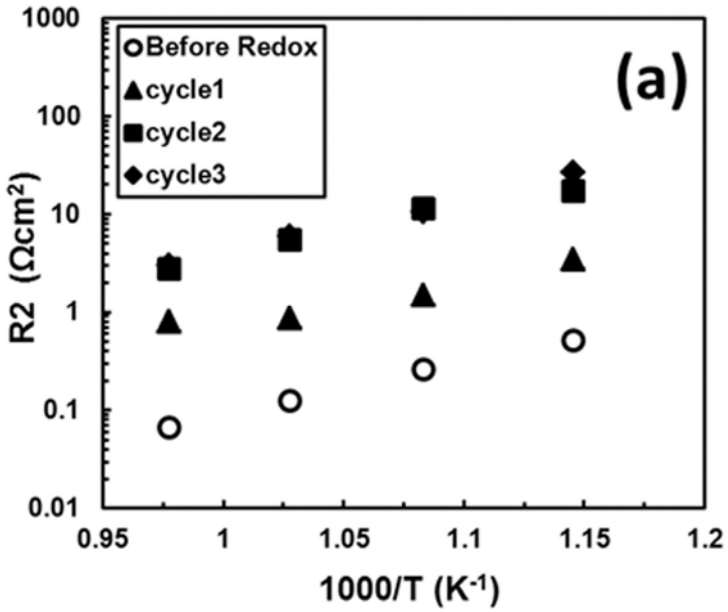
Before Redox
cycle1
cycle2
cycle3
(a)
R2 (Ωcm²)
1000/T (K⁻¹)
1000
100
10
1
0.1
0.01
0.95
1
1.05
1.1
1.15
1.2

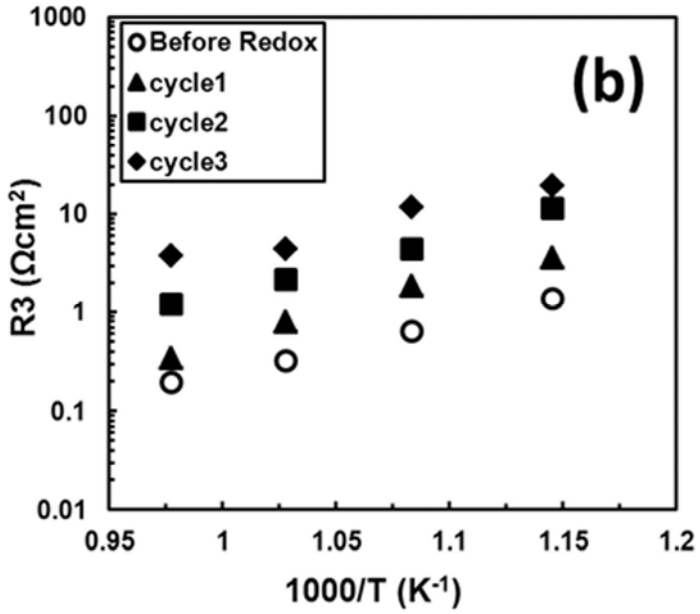
Before Redox
cycle1
cycle2
cycle3
(b)
R3 (Ωcm²)
1000/T (K⁻¹)
1000
100
10
1
0.1
0.01
0.95
1
1.05
1.1
1.15
1.2

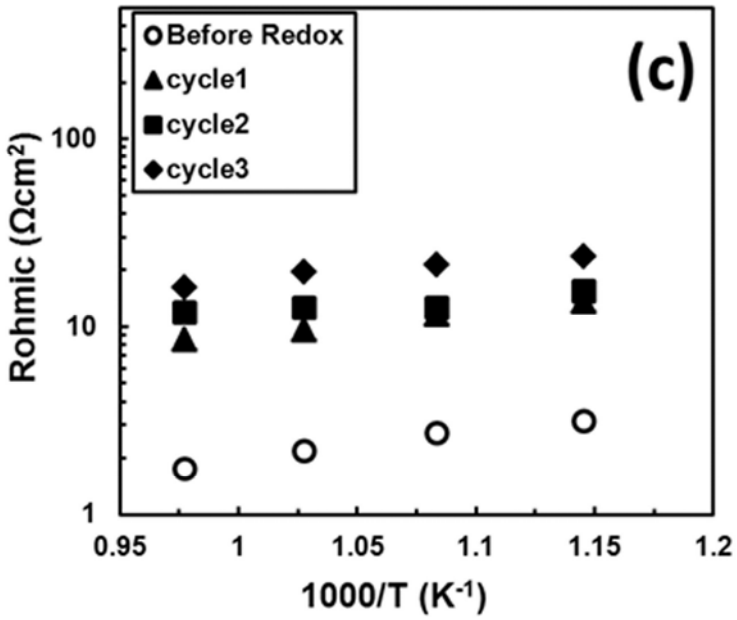

Figure 8: The effect of redox cycling on (a) High frequency polarization resistance R2, (b) low frequency polarization resistance R3 and (c) ohmic resistance Rohmic as a function of temperature for 40 vol% Ni-BZY cermet anode measured in wet 10% H_2/N_2 and air.

To put these results into context, Figure 9 plot the percentage change in the values of the polarization resistances R2 and R3 and the ohmic resistance Rohmic as a function of number of redox cycles, given by the equation

$$\Delta R\% = 100.\frac{R_i^{//} - R_i^{/}}{R_i^{/}} \qquad (2)$$

where $R_i^{/}$ and $R_i^{//}$ are the resistances before and after redox cycling, respectively, of any resistance component i The most severe degradation issues are manifested by the polarization resistances R2 and R3. Both these terms demonstrate performance impairments of up to 100% that of the initial resistance after a few redox cycles. Large degradation issues are also shown by the ohmic resistance, where diminished interfacial contacts produce a performance depletion that is approximately 80% of the original resistance upon redox cycling. The most perturbing feature of Fig. 9 is the extremely rapid depletion of each of these electrochemical terms. A single redox event is shown to

be able to impair the polarization and interfacial resistances of peak performing PCFC cermet anodes, producing performance decreases that correspond to at least 80% of the original resistance values. The severity of this degradation highlights the conundrum facing state of the art PCFC anodes; the low porosity desirable for high electrochemical performance is likely to be contrary to that required for high redox stability. It is, therefore, imperative that innovative methods to circumvent this impasse are proposed by the protonics community.

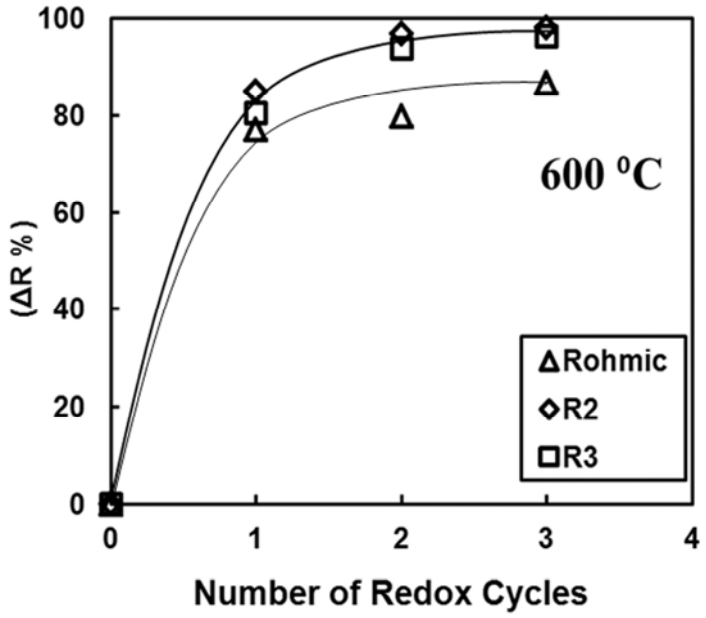

Figure 9: The percentage change in the high frequency polarization resistance, R2, the low frequency polarization resistance, R3, and the ohmic resistance, Rohmic, as a function of redox cycling for 40 vol% Ni-BZY cermet anode measured at 600 ºC.

4. Conclusions

The redox cycling behavior of Ni-BZY anodes for PCFCs were investigated by using electrochemical impedance measurements under 10% H_2/N_2 gas mixture and air. The impedance spectra show that both the high frequency semi-circle, R2, and the low frequency semi-circle, R3, were increased by re-oxidation and reduction cycles. The ohmic resistance (Rohmic) was also increased due to delamination at anode/electrolyte

interface, as confirmed by SEM analysis after redox cycling. The formation of microcracks in the cermet BZY oxide network and across the symmetrical cell was also observed upon redox cycling. ESEM analysis highlights that these microcracks and delamination form due to the volume expansion of the Ni cermet phase upon re-oxidation. As such, a rapid depletion in performance is observed in peak performing PCFC anodes of low porosity upon redox cycling, despite their high initial connectivity and the potential for proton migration in both cermet phases. This result can be considered to be highly detrimental to practical exploitation of PCFCs. Thus, the study of methods to minimise this factor can be considered to be imperative before PCFCs may become commercially feasible.

.

Acknowledgements

The authors gratefully acknowledge the funding from the FCT, FEDER, COMPETE, PTDC/CTM/100412/2008, PTDC/CTM/105424/2008, and Narendar Nasani thankful to FCT for doctoral research grant SFRH/BD/80949/2011.

References

[1] Stambouli AB, Traversa E. Solid oxide fuel cells (SOFCs): a review of an environmentally clean and efficient source of energy. Renewable Sustainable Energy Rev. 2002;6:433–55.
[2] Orera A, Slater PR. New Chemical Systems for Solid Oxide Fuel Cells†. Chem Mater. 2010;22:675-90.
[3] Fabbri E, Pergolesi D, Traversa E. Materials challenges toward proton-conducting oxide fuel cells: a critical review. Chem Soc Rev. 2010;39:4355-69.
[4] Fabbri E, Pergolesi D, Traversa E. Electrode materials: a challenge for the exploitation of protonic solid oxide fuel cells. Sci Technol Adv Mater. 2010;11:044301.
[5] Chevallier L, Zunic M, Esposito V, Di Bartolomeo E, Traversa E. A wet-chemical route for the preparation of Ni–$BaCe_{0.9}Y_{0.1}O_{3-\delta}$ cermet anodes for IT-SOFCs. Solid State Ionics. 2009;180:715-20.
[6] Zunic M, Chevallier L, Radojkovic A, Brankovic G, Brankovic Z, Di Bartolomeo E. Influence of the ratio between Ni and $BaCe_{0.9}Y_{0.1}O_{3-\delta}$ on microstructural and electrical properties of proton conducting Ni–$BaCe_{0.9}Y_{0.1}O_{3-\delta}$ anodes. J Alloys Compd. 2011;509:1157-62.
[7] Bi L, Fabbri E, Sun Z, Traversa E. $BaZr_{0.8}Y_{0.2}O_{3-\delta}$-NiO Composite Anodic Powders for Proton-Conducting SOFCs Prepared by a Combustion Method. J Electrochem Soc. 2011;158:B797.
[8] Rainwater BH, Liu M, Liu M. A more efficient anode microstructure for SOFCs based on proton conductors. Int J Hydrogen Energy. 2012;37:18342-8.
[9] Mather GC, Figueiredo FM, Fagg DP, Norby T, Jurado JR, Frade JR. Synthesis and characterisation of Ni–$SrCe_{0.9}Yb_{0.1}O_{3-\delta}$ cermet anodes for protonic ceramic fuel cells. Solid State Ionics. 2003;158:333-42.
[10] Mather GC, Figueiredo FM, Jurado JR, Frade JR. Synthesis and characterisation of cermet anodes for SOFCs with a proton-conducting ceramic phase. Solid State Ionics. 2003;162-163:115-20.
[11] Zuo C, Lee TH, Dorris SE, Balachandran U, Liu M. Composite Ni–$Ba(Zr_{0.1}Ce_{0.7}Y_{0.2})O_3$ membrane for hydrogen separation. J Power Sources. 2006;159:1291-5.
[12] Sun W, Yan L, Shi Z, Zhu Z, Liu W. Fabrication and performance of a proton-conducting solid oxide fuel cell based on a thin $BaZr_{0.8}Y_{0.2}O_{3-\delta}$ electrolyte membrane. J Power Sources. 2010;195:4727-30.
[13] Coors WG, Manerbino A. Characterization of composite cermet with 68wt.% NiO and $BaCe_{0.2}Zr_{0.6}Y_{0.2}O_{3-\delta}$. J Membr Sci. 2011;376:50-5.
[14] Zuo C, Dorris SE, Balachandran U, Liu M. Effect of Zr-Doping on the Chemical Stability and Hydrogen Permeation of the Ni-$BaCe_{0.8}Y_{0.2}O_{3-\alpha}$ Mixed Protonic-Electronic Conductor. Chem Mater. 2006;18:4647-50.
[15] Narendar N, Mather GC, Dias PAN, Fagg DP. The importance of phase purity in Ni–$BaZr_{0.85}Y_{0.15}O_{3-\delta}$ cermet anodes – novel nitrate-free combustion route and electrochemical study. RSC Adv. 2013;3:859-69.
[16] Ettler M, Timmermann H, Malzbender J, Weber A, Menzler NH. Durability of Ni anodes during reoxidation cycles. J Power Sources. 2010;195:5452-67.
[17] Coors WG. Protonic ceramic steam-permeable membranes. Solid State Ionics. 2007;178:481-5.

[18] Laurencin J, Delette G, Sicardy O, Rosini S, Lefebvre-Joud F. Impact of 'redox' cycles on performances of solid oxide fuel cells: Case of the electrolyte supported cells. J Power Sources. 2010;195:2747-53.
[19] Zhang Y, Liu B, Tu B, Dong Y, Cheng M. Understanding of redox behavior of Ni–YSZ cermets. Solid State Ionics. 2009;180:1580-6.
[20] Sarantaridis D, Atkinson A. Redox Cycling of Ni-Based Solid Oxide Fuel Cell Anodes: A Review. Fuel Cells. 2007;7:246-58.
[21] Klemensø T, Chung C, Larsen PH, Mogensen M. The Mechanism Behind Redox Instability of Anodes in High-Temperature SOFCs. J Electrochem Soc. 2005;152:A2186.
[22] Klemensø T, Mogensen M. Ni–YSZ Solid Oxide Fuel Cell Anode Behavior Upon Redox Cycling Based on Electrical Characterization. J Am Ceram Soc. 2007;90:3582-8.
[23] Heo Y-H, Lee J-W, Lee S-B, Lim T-H, Park S-J, Song R-H, et al. Redox-induced performance degradation of anode-supported tubular solid oxide fuel cells. Int J Hydrogen Energy. 2011;36:797-804.
[24] Laurencin J, Delette G, Morel B, Lefebvre-Joud F, Dupeux M. Solid Oxide Fuel Cells damage mechanisms due to Ni-YSZ re-oxidation: Case of the Anode Supported Cell. J Power Sources. 2009;192:344-52.
[25] Baek S-W, Bae J. Anodic behavior of $8Y_2O_3$–ZrO_2/NiO cermet using an anode-supported electrode. Int J Hydrogen Energy. 2011;36:689-705.
[26] Coors WG. Protonic ceramic fuel cells for high-efficiency operation with methane. J Power Sources. 2003;118:150-6.
[27] Narendar N, Devaraj R, Brandão A, Yaremchenko A, Fagg DP. The impact of porosity, pH_2 and pH_2O on the polarisation resistance of Ni-$BaZr_{0.85}Y_{0.15}O_{3-\delta}$ cermet anodes for Protonic Ceramic Fuel Cells (PCFCs). Int J Hydrogen Energy (Submitted).
[28] Pihlatie M, Ramos T, Kaiser A. Testing and improving the redox stability of Ni-based solid oxide fuel cells. J Power Sources. 2009;193:322-30.
[29] Antunes I, Brandão A, Figueiredo FM, Frade JR, Gracio J, Fagg DP. Mechanosynthesis of nanopowders of the proton-conducting electrolyte material Ba(Zr, Y)$O_{3-\delta}$. J Solid State Chem. 2009;182:2149-56.
[30] Nasani N, Dias PAN, Saraiva JA, Fagg DP. Synthesis and conductivity of Ba(Ce,Zr,Y)$O_{3-\delta}$ electrolytes for PCFCs by new nitrate-free combustion method. Int J Hydrogen Energy. 2013;38:8461-70.
[31] Atkins P, de Paula J. Physical Chemistry: Thermodynamics And Kinetics. 8th ed. New York: W.H. Freeman; 2006.
[32] Faes A, Hessler-Wyser A, Zryd A, Van herle J. A Review of RedOx Cycling of Solid Oxide Fuel Cells Anode. Membranes. 2012;2:585-664.
[33] Essoumhi A, Taillades G, Taillades-jacquin M, Jones D, Roziere J. Synthesis and characterization of Ni-cermet/proton conducting thin film electrolyte symmetrical assemblies. Solid State Ionics. 2008;179:2155-9.
[34] Zhao F, Virkar AV. Dependence of polarization in anode-supported solid oxide fuel cells on various cell parameters. J Power Sources. 2005;141:79-95.